Preprints of the 21st IFAC World Congress (Virtual)
Berlin, Germany, July 12-17, 2020

Sensor network design for smart manufacturing – Application on precision machining ⋆

Utsav Awasthi * **George M. Bollas** *

* *Department of Chemical & Biomolecular Engineering, UTC Institute for Advanced Systems Engineering, University of Connecticut, 159 Discovery Dr, Storrs, CT, 06269, USA (e-mail: {utsav.awasthi; george.bollas}@uconn.edu)*

Abstract: Energy consumption in a manufacturing facility comprises direct energy used in the manufacturing operations and indirect energy consumed by activities to maintain proper equipment conditions (e.g., heating and cooling). Reducing the energy consumption in a manufacturing facility requires sensors to monitor the energy usage patterns ("energy profiles") and a concomitant data analytics process for correlating them with the activities being performed. This work explores the design and integration of optimal sensor networks for measuring and identifying the context of energy usage in manufacturing processes. This information is useful in production planning and scheduling to optimize energy usage and reduce energy cost. We explore a system-level representation of precision machining for optimal sensor locations and types that allow the monitoring of energy consumption. This is accomplished through maximization of a measure of the information matrix, subject to constraints on the cost of sensors. First, a system-level model is presented for predicting energy consumption in precision machining. A formulation is then presented for the selection of sensors and the operating mode for maintenance tests in manufacturing. The sensor network design is cast as a mixed-integer non-linear program that selects possible sensors based on their contribution to information gain with respect to energy consumption and their impact on equipment cost. For this purpose, we explore the sensitivity of the machining process with respect to admissible inputs at different system fault scenarios.

Keywords: Energy control, energy management systems, manufacturing systems, optimization, sensor network.

1 Introduction

Subtractive manufacturing involves removal of material to produce a finished work piece through milling, drilling performed by Computer Numerical Control (CNC) machines. Machining processes in general are highly energy intensive. A large fraction of the electrical energy consumed in the manufacturing industry is due to machining operations. According to the U.S. Energy Information Administration (US Energy Information Administration, 2011), 75 % of the total electricity consumed in industry is due to machining operations, as shown in Fig. 1.

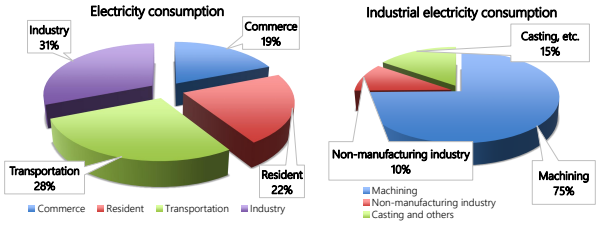

Fig. 1. Energy consumption by machining process

Gutowski et al. (2006) categorized the energy consumed in 3-axis milling into three categories: start-up, constant run time, and variable with respect to load. According to their study, 65.8 % of the total energy consumed in machining is attributed to the milling operation. Modeling of machining can provide insights into energy consumption and enable model-based control architectures for these systems. Moradnazhad and Unver (2017) presented a comprehensive review on modeling of the energy consumption

⋆ This material is based upon work supported by the U.S. Department of Energy's Office of Energy Efficiency and Renewable Energy (EERE) under the Advanced Manufacturing Office Award Number DE-EE0007613.

in machining. The focus of this work is to present a framework that utilizes these physics-based models in order to find maintenance test settings and sensor networks for improved sensing of machine state and malfunctions in precision machining. The first step in designing these tests is to explore the impact of faults and malfunctions on the machining power consumption using a validated model. To accomplish this goal, a model of the power consumption in a face milling machine is formulated on the basis of the work of Shao et al. (2004). Model inputs, parameters and outputs are identified and a fault detection and isolation methodology is proposed based on Awasthi et al. (2020).

2 Machining Model

The energy model for precision machining developed by Shao et al. (2004) is used to compute power consumption and explore the sensitivity of power consumption with respect to system parameters and admissible inputs. The model was augmented with the cutting fluid utilization and scrap generation models of Munoz and Sheng (1995).

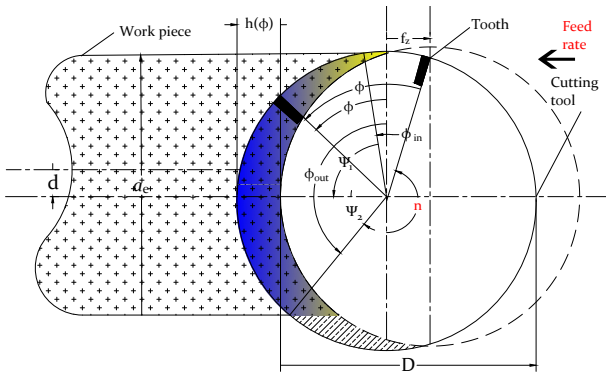

Fig. 2. Sketch of machining process for the calculation of power consumption.

2.1 Power consumption

Fig. 2 shows a sketch of the machining process. The power consumption is determined by the tangential component of the cutting force. Then, computation of the milling force is used to calculate power consumption.

2.1.1 Force of milling: Consider a tool of diameter D with number of teeth Z, that chips the work piece with a width of cut a_e. The immersion angle ψ is determined by the portion of the work piece that the tool is acting on, a_e. This immersion angle is divided horizontally into two components ψ_1 and ψ_2 ($\psi = \psi_1 + \psi_2$), computed by Eqs. (1–2), where δ is the offset distance between the cutter center and the work piece.

$$\psi_1 = \arcsin\left[(a_e + 2\delta)/D\right], \tag{1}$$

$$\psi_2 = \arcsin\left[(a_e - 2\delta)/D\right], \tag{2}$$

The tangential force for cutting is calculated by using the force equation, Eq. (3), proposed by Altintas (1988). The instantaneous angle of a tooth with the normal to the direction of tool motion is represented by ϕ:

$$F_t(\phi) = a_p[K\bar{h}^{-c} f_z \sin\phi], \tag{3}$$

$$\phi_{in} = \pi/2 - \psi_1, \quad \phi_{out} = \pi/2 + \psi_2 \tag{4}$$

where ϕ_{in} is the the angle made by the cutting zone with the normal to the direction of motion of the tool and ϕ_{out} is the exit angle of the tool from the work piece. The mean chip thickness $\bar{h}$ is computed by Eq. (5), where f_z is the feed per tooth:

$$\bar{h} = \frac{f_z}{\psi}(\sin\psi_1 + \sin\psi_2), \quad f_z = \frac{f}{nZ}. \tag{5}$$

Tool wear takes place during the cutting process. The force from flank wear was presented in Waldorf et al. (1992), in terms of two force components: (i) force normal to the wear land; and (ii) force because of friction. The net tangential component of the force takes into account the total force needed to cut the work piece and the force from tool wear:

$$F_t(\phi) = a_p[K\bar{h}^{-c} f_z \sin\phi + \mu H\overline{VB}], \tag{6}$$

where K is the cutting force constant, c is the chip thickness constant computed experimentally, μ is the friction coefficient, H is the material hardness, and $\overline{VB}$ is the average flank wear land width.

2.1.2 Power consumption: Using Eq. (6), the cutting power for the i-th tooth can be computed as:

$$p_i(\phi) = \pi D n F_t(\phi) \qquad \forall \ \phi \in [\phi_{in}, \phi_{out}], \tag{7}$$

where n is the spindle speed calculated form the cutting speed ν and diameter of spindle D, and i is the number of teeth ($i = 1, ..., m, ..., Z$):

$$n = \frac{\nu 1000}{\pi D} \tag{8}$$

In the milling operation usually multiple teeth are involved simultaneously in cutting. Let m teeth be simultaneously involved in the milling process. The maximum value of m can be $Z/2$ when the tool is in full immersion. The power of cutting can then be divided into two phases (Shao et al. (2004)): (i) phase A, where m teeth are involved in cutting; (ii) phase B, where $m-1$ teeth are involved in the cutting process. Thus, the power of cutting for the j-th cutting cycle can be computed by Eq. (9):

$$P_j(\phi) = \begin{cases} \sum_{i=1}^{m} p_i(\phi) \\ \sum_{i=1}^{m-1} p_i(\phi) \end{cases} \tag{9}$$

P_m in Eq. (9) can be further expanded and the expression for power is given by Eq. (10):

$$P_j(\phi) = \begin{cases} P_m(\phi), \\ (\phi_{in} + (j-1)\Phi) \\ \qquad \leq \phi < (\psi + \phi_{in} + (j-m)\Phi) \\ P_{m-1}(\phi), \\ (\psi + \phi_{in} + (j-m)\Phi) \\ \qquad \leq \phi < (\phi_{in} + j\Phi) \end{cases}, \tag{10}$$

where $j = 1, 2, 3, ..., N$, and P_m is computed by Eq. (11), with K and c constants computed experimentally and m the number of teeth involved in cutting simultaneously:

$$P_m(\phi) = \pi D n a_p \Big[K\bar{h}^{-c} f_z \frac{\sin(\phi + (m-1)\Phi/2)\sin(m\Phi/2)}{\sin(\Phi/2)} + \mu H m \overline{VB} \Big] \tag{11}$$

Eq. (12) is then obtained by integrating Eq. (7) from ϕ_{in} to ϕ_{out} to calculate the mean cutting power consumption for the face milling operation:

$$\overline{P} = ZnDa_p[K\bar{h}^{-c}f_z(\cos(\phi_{in}) - \cos(\phi_{in} + \psi))+ \mu H\overline{VB}\psi]/2 \quad (12)$$

Eq. (12) is used to compute the mean power as a function of cutting speed ν and feed rate f, which are admissible inputs in the machining process. The parameters in this power consumption model are the number of teeth of the cutter Z, cutter diameter D, cutting force constant K, chip thickness constant c, number of teeth simultaneously involved in cutting m, width of cut a_e, depth of cut a_p and material hardness H. For calculating the mean cutting power at any one instance of machining, $\overline{VB}$, can be considered constant, while μ was also assumed constant in Shao et al. (2004), when cutting fluid is not used. For simplicity we consider μ to be constant, but its value depends on the forces acting between the tool and the work piece. Both instantaneous power, Eq. (10), and mean cutting power, Eq. (12), can thus be computed as functions of machining parameters and input variables.

2.2 Scrap generation

In the milling process, scrap generation results in loss of material. Scrap generation is a separate problem altogether with models aiming to reduce the amount of scrap and rework. Eq. (13) gives the formulation for scrap generation in a cut with width a_e and depth a_p:

$$V_{scrap} = a_e a_p f \quad (13)$$

The total scarp generation is the difference of volumes of the initial work piece, V_i, and finished work piece, V_f:

$$\overline{V}_{scarp} = V_f - V_i, \quad (14)$$

2.3 Cutting fluid loss

Cutting fluid is often utilized in machining to provide lubrication, and control overheating of the work piece. High-speed machining results in temperature increase of the work piece and tool which can distort the work piece or tool piece. This might cause an increase in scarp generation or tool breakage. The total amount of cutting fluid needed for the machining process is the sum of the loss of cutting fluid because of sticking of fluid to the chips, fluid loss due evaporation of cutting fluid, amount of cutting fluid that is recirculated, and the amount of cutting fluid because of coating on the work piece (Munoz and Sheng, 1995). Cutting fluid loss and the associated energy penalty is not considered in detail here and is the subject of current work.

3 Manufacturing Conditions and Sensor Selection

The machining power consumption model is first written as the set of differential algebraic equations of Eq. (15), where $\mathbf{f}$ is the system governing equations, $\mathbf{x}(t)$ is the vector of state variables, $\mathbf{u}(t)$ is the vector of admissible inputs, $\boldsymbol{\theta}$ is the vector of model parameters, and t is the time. Eq. (15) is valid for a timespan, τ, during which all model parameters remain invariant:

$$\mathbf{f}(\dot{\mathbf{x}}(t), \mathbf{x}(t), \mathbf{u}(t), \boldsymbol{\theta}, t) = \mathbf{0}. \quad (15)$$

The formulation of dynamic test designs is presented in Palmer and Bollas (2019b). In the application presented here, the system is considered at steady-state. Therefore, the terms $\dot{\mathbf{x}}$ and t are removed. The measurable output vector, $\hat{\mathbf{y}}$, is a function of states, inputs and parameters as shown in Eq. (16):

$$\hat{\mathbf{y}} = \mathbf{h}(\mathbf{x}, \mathbf{u}, \boldsymbol{\theta}). \quad (16)$$

Each variable that corresponds to a potential sensor available in the manufacturing system is listed as an output. Thus, $\hat{\mathbf{y}}$ is considered to have N_y elements. A subset of sensors is to be selected from the potential N_y sensors. This set is desired to contain maximum information with respect to the state of the manufacturing system. This results in a combinatorial problem with respect to sensor selection, where the N_y available or potential sensors are split into n_y selected sensors ($n_y \in 1, \ldots, N_y$) and $N_y - n_y$ dormant sensors. These decisions are formulated mathematically by introducing a binary vector, $\mathbf{a}$. Each element in $\mathbf{a}$ activates or deactivates a specific measured element in $\hat{\mathbf{y}}$; it assigns a value of 0 for when a sensor is not used, or 1 for when it is active.

The input trajectories are divided into two subvectors that represent controllable process inputs, $\mathbf{u}_p$, and uncertainty upstream to the system, $\mathbf{u}_u$:

$$\mathbf{u} = [\mathbf{u}_p, \mathbf{u}_u]. \quad (17)$$

$\mathbf{u}_p$ is the matrix of N_u inputs for N_{test} operating modes, hence $\mathbf{u}_p \in \mathbb{R}^{N_u \times N_{test}}$. The operating envelop (design vector) for $\mathbf{u}_p$ may be continuous ($\mathbf{u}_p^L \leq \mathbf{u}_p \leq \mathbf{u}_p^U$) or discrete. In the discrete case, a finite number, N_d, of operating modes (steady state or transient operating conditions that are the result of a set of settings for the inputs or input trajectories) are available for manufacturing state diagnosis. Thus, in the case of finite discrete test settings N_d, if N_{test} test designs are to be selected for the optimization then $\mathbf{u}_p \in \mathbb{R}^{N_u \times N_{test}}$ needs to be selected from the set $\mathbf{U}_p \in \mathbb{R}^{N_u \times N_d}$, $N_{test} \leq N_d$. For the machining process, the inputs are the cutting speed, ν, and the feed rate, f, which is defined by the depth of cut, a_e.

The system parameters are divided into three subvectors: parameters that represent faults, $\boldsymbol{\theta}_f$, parameters that represent system uncertainty, $\boldsymbol{\theta}_u$, and parameters that represent system design and are known and invariant, $\boldsymbol{\theta}_p$:

$$\boldsymbol{\theta} = [\boldsymbol{\theta}_f, \boldsymbol{\theta}_u, \boldsymbol{\theta}_p]. \quad (18)$$

Table 1 provides the list of parameters in the machining process, as identified in the previous section. The uncertain parameters can be the metal hardness, H, of the work piece on which the tool is working. Thermal deformation and deformation under cutting forces result in uncertainty in the depth of cut, a_p and width of cut, a_e. The parameter that represents fault is the amount of tool that has worn out represented by average flank wear width $\overline{VB}$.

The faults and uncertain parameters and inputs of Table 1 are compiled into a vector that can be optimized for sensor and manufacturing mode selection for machine state identification:

$$\boldsymbol{\xi} = [\boldsymbol{\theta}_f, \boldsymbol{\theta}_u, \mathbf{u}_u]. \quad (19)$$

The system faults are selected as targets for identification and diagnosis, therefore the elements of $\boldsymbol{\xi}$ are separated into faults and system uncertainty. The vector $\boldsymbol{\xi}$ is partitioned to $\boldsymbol{\xi} = [\xi_1, ..., \xi_{N_f}, \xi_{N_{f+1}}, , ..., \xi_{N_\xi}] = [\boldsymbol{\xi}_f, \boldsymbol{\xi}_u]$, where

Table 1. System inputs, outputs and parameters

Inputs, $\mathbf{u}_p$	
n	Spindle speed
f	Feed rate
Outputs, $\mathbf{y}$	
$\bar{P}$	Mean Cutting Power
V_{scrap}	Scrap generation
Parameters, θ_p	
Z	Number of teeth
D	Diameter of milling cutter
δ	Offset distance between work piece and tool
V_i	Initial volume of work piece
V_f	Final volume of the work piece
T_{amb}	Ambient temperature
T_{vap}	Vaporization temperature of cutting fluid
L	Latent heat of vaporization
c_p	Specific heat of cutting fluid
l	Chip contact length
l_m	Major length scale of the work piece
$\bar{p}_i$	Idle-running power of a spindle motor
μ	Friction coefficient
Uncertainty, $\boldsymbol{\xi}_u$	
a_p	Depth of cut
a_e	Width of cut
H	Material hardness
Faults, $\boldsymbol{\xi}_f$	
$\overline{VB}$	Average flank land wear width

$\boldsymbol{\xi}_f$ is the vector of N_f parameters representing faults, $\boldsymbol{\xi}_u$ is the vector of remaining elements of $\boldsymbol{\xi}$ that represent system uncertainty. The anticipated faults and uncertainty vector (mean values) at fault f are represented by $\tilde{\boldsymbol{\xi}}_f \in \boldsymbol{\Xi}$, where $f = 1, ..., N_f$ and $\boldsymbol{\Xi} \in \mathbb{R}^{N_f \times N_\xi}$, with rows containing the fault parameter values for each fault scenario, c^f, $f = 1, ..., N_f$. Thus, $\boldsymbol{\Xi}$ represents the matrix of all anticipated values of uncertainty and faults that are predefined for the system. By representing faults as system parameters the method deals with abrupt or incipient faults that are persistent, known and anticipated in the test timespan.

The problem of sensor and manufacturing mode selection for state identification is cast as an optimization that maximizes some measure of the Fisher Information Matrix (FIM) (Palmer and Bollas, 2019a). If we consider system uncertainty that does not correspond to faults as nuisance model parameters, the objective of the test design then becomes a maximization of the sensitivity of outputs with respect to faults and a minimization of the correlation between these faults and the impact of system uncertainty in fault diagnosis. Here, Fisher information is used as a metric of the identifiability of faults for a certain operating mode and with a certain set of sensors. These faults are treated as a subset of uncertain parameters of a high-fidelity model of the system of interest. The task of manufacturing state identification test design and sensor selection then becomes an exercise of determining tests that simultaneously maximize the evidence of faults on outputs, minimizes the correlation between multiple faults and uncertainty and minimizes the effect of uncertainty on outputs, for a given model structure. This is accomplished using the model of the previous section and calculating its so-called Fisher Information Matrix, FIM. The FIM is cast as a function of sensitivities, calculated as partial derivatives of outputs with respect to faults and uncertainty. For steady-state FDI, these sensitivities are compiled into a matrix, $\mathbf{Q}_{if}^{[k]}$, for each output i and test design k and fault f. The size of $\mathbf{Q}_{i,f}^{[k]}(\boldsymbol{\varphi}, \tilde{\boldsymbol{\xi}}_f)$ is N_ξ as shown in Eq. (20):

$$\mathbf{Q}_{i,f}^{[k]} = \left[\left. \frac{\partial \hat{y}_i(\mathbf{u}_p^{[k]})}{\partial \xi_1} \right|_{\tilde{\boldsymbol{\xi}}_f} \cdots \left. \frac{\partial \hat{y}_i(\mathbf{u}_p^{[k]})}{\partial \xi_{N_\xi}} \right|_{\tilde{\boldsymbol{\xi}}_f} \right]. \tag{20}$$

In Eq. (20), $\tilde{\boldsymbol{\xi}}$ is the matrix of the anticipated fault and uncertainty values for which the test is designed. This matrix ($N_f \times N_\xi$ dimension) populates all the possible fault scenarios for which $\mathbf{Q}_{i,f}^{[k]}$ needs to be calculated. These scenarios are summed in Eq. (21), where the sensitivity matrices are used to compute the FIM, $\mathbf{H}_\xi$:

$$\mathbf{H}_\xi(\boldsymbol{\varphi}, \tilde{\boldsymbol{\xi}}) = \sum_{f=1}^{N_f} \sum_{k=1}^{N_{test}} \sum_{i=1}^{N_y} \sum_{j=1}^{N_y} a_i a_j \sigma_{ij}^{-2} \mathbf{Q}_{i,f}^{[k]^T} \mathbf{Q}_{j,f}^{[k]}, \tag{21}$$

where σ_{ij}^2 is the measurement variance of the i-th and j-th outputs. Each element of $\mathbf{a}$ in Eq. (21) corresponds to the i-th and j-th outputs. Eq. (21) can be normalized for the number of sensors of each design to weigh the benefit of additional test information with the expense of sensing infrastructure (Palmer and Bollas, 2019; Palmer et al., 2019). The normalized FIM is shown in Eq. (22):

$$\bar{\mathbf{H}}_\xi(\boldsymbol{\varphi}, \tilde{\boldsymbol{\xi}}) = \frac{\sum_{f=1}^{N_f} \sum_{k=1}^{N_d} \sum_{i=1}^{N_y} \sum_{j=1}^{N_y} a_i a_j \sigma_{ij}^{-2} \mathbf{Q}_{i,f}^{[k]^T} \mathbf{Q}_{j,f}^{[k]}}{\sum_{i=1}^{N_y} a_i}, \tag{22}$$

where $\sum_{i=1}^{N_y} a_i$ is the normalization factor, expressed as the summation of the sensors that contribute to a particular sensor network design. The manufacturing test design vector, $\boldsymbol{\varphi}$, is compiled from continuous and/or discrete variables and is adjusted to improve the quality of a manufacturing health test. The vector consists of the binary vector $\mathbf{a}$ and the input test settings $\mathbf{u}_p$. The design vector must be within the test design space $\boldsymbol{\Phi}$, defined by the machine limits. The design vector is then expressed as $\boldsymbol{\varphi} = [\mathbf{u}_p, \mathbf{a}] \in \boldsymbol{\Phi}$. The D_s-optimality criterion (Atkinson and Bogacka, 1997) was selected for its ability to reduce the joint confidence region for a target set of parameters in the presence of other uncertain parameters. In D_s-optimal design, the FIM is partitioned into submatrices, corresponding to the faults, $\boldsymbol{\xi}_f$, and the uncertainty, $\boldsymbol{\xi}_u$. The submatrices are classified as $\boldsymbol{H}_{ff}$, $\boldsymbol{H}_{fu}$ and $\boldsymbol{H}_{uu}$ to represent the covariance between faults, between faults and system uncertainty and between system uncertainty, respectively. The criterion is then calculated as:

$$\Psi_{Ds}(\mathbf{H}_\xi) = \left| (\boldsymbol{H}_{ff} - \boldsymbol{H}_{fu} \boldsymbol{H}_{uu}^{-1} \boldsymbol{H}_{fu}^T) \right|, \tag{23}$$

The optimization problem for the steady-state test design out of a continuous set of machining operating modes is:

$$\begin{aligned} \boldsymbol{\varphi}^* \in \arg \max_{\boldsymbol{\varphi} \in \Phi} & \ln \left(\Psi_{Ds} \left(\mathbf{H}_\xi(\tilde{\boldsymbol{\xi}}, \boldsymbol{\varphi}) \vee \bar{\mathbf{H}}_\xi(\tilde{\boldsymbol{\xi}}, \boldsymbol{\varphi}) \right) \right) \\ \text{s.t.} & \\ & \mathbf{f}(\mathbf{x}, \mathbf{u}_p, \boldsymbol{\theta}_p, \tilde{\boldsymbol{\xi}}) = \mathbf{0}, \\ & \hat{\mathbf{y}} = \mathbf{h}(\mathbf{x}, \mathbf{u}_p, \boldsymbol{\theta}_p, \tilde{\boldsymbol{\xi}}) \\ & \mathbf{u}_p^L \le \mathbf{u}_p \le \mathbf{u}_p^U, \\ & \mathbf{x}^L \le \mathbf{x} \le \mathbf{x}^U. \end{aligned} \tag{24}$$

Table 2. Experimental conditions (Shao et al., 2004)

Work piece	Material: Cast Iron H = 1689 N/m Size = 500 x 70 x 500
Cutter	Material: Carbide Number of teeth= 1 and 5 Diameter = 100 mm
Cutting condition	Depth of cut: 2 - 6 mm Feed: 0.065-2 mm/rev Cutting speed: 18-236 m/min Width of cut: 70 mm Offset distance: 0 Cut type: Up and down milling

The optimization problem formulated above determines the optimal design (sensors and test settings), when the machining modes comprise a continuous set. This is not very common, so the problem was reformulated to determine optimal test settings out of a discrete set of operating modes. The corresponding formulation is identical to that of Eq. (24), but with $\mathbf{u}_p \subset \mathbf{U}_p$, where $\mathbf{U}_p \in \mathbb{R}^{N_u \times N_d}$. The solution of Eq. (24) gives the D_s-optimal test design that consists of N_{test} test settings and n_y sensors that maximize the sensitivity of outputs with respect to faults and minimizes joint confidence between faults and uncertainty.

4 Results and Discussion

4.1 Model Validation

The power consumption for precision machining described earlier was validated against data from Shao et al. (2004) for a face milling process involving one tooth or five teeth. The reference data used are listed in Table 2 with cutting conditions listed in detail in Table 3. The data and results of the model by Shao et al. (2004) were reproduced using the power consumption model for single tooth milling, $Z = 1$, and multiple teeth milling, $Z = 5$, and compared to the experimental measurements of power consumption. The mean power consumption was calculated for a work piece with initial volume V_i and final volume of V_f. Figs. 3–4 present the model predictions for the cases studied. In the study by Shao et al. (2004) cutting fluid was not considered; thus, μ was considered to be constant at its reference value (Shao et al., 2004). Overall, the power consumption model was validated with the literature data and was found to be in excellent agreement. We then proceeded to exploring the dependency of the power consumption on system admissible inputs as a function of tool wear, which in the presented framework was considered a fault.

4.2 Sensitivity Analysis

The correlation between power consumption with cutting speed, depth of cut and feed rate was computed for the machining process for two tool wear, $\overline{VB}$, cases. The two tool wear criteria used in the sensitivity analysis is $\overline{VB} = 0$ mm for a new tool and $\overline{VB} = 3$ mm for a worn out tool. The significance of each of the manufacturing decision variables on power consumption at these different tool wear values was first assessed using sensitivity analysis. Table 4 shows the values of the inputs used to define the design vector of the manufacturing maintenance test. In

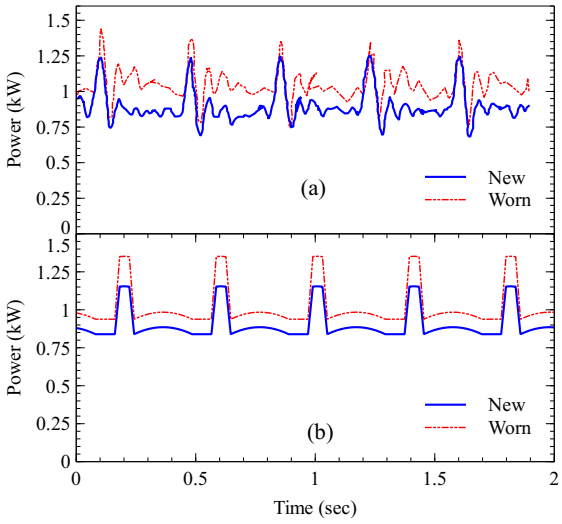

Fig. 3. Power consumption for single tooth milling operation for new and worn tool. (a) data from Shao et al. (2004); (b) model predictions.

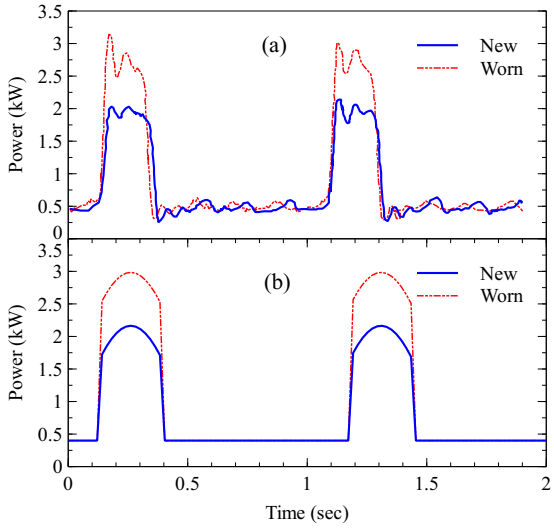

Fig. 4. Power consumption for multiple tooth milling operation for new and worn tool. (a) data from Shao et al. (2004); (b) model predictions.

the sensitivity analysis, each process was varied with mean values for all other machining parameters and the other two inputs set at their mean values. The sensitivities are presented as plots of $\partial\overline{P}/\partial\nu$ for the sensitivity of power consumption with respect to cutting speed ν, $\partial\overline{P}/\partial a_p$ for the sensitivity of power consumption with respect to depth of cut a_p and $\partial\overline{P}/\partial f$ for the sensitivity of power consumption with respect to feed rate f. These sensitivities along with the value of power consumption are plotted against the three inputs for the two tool wear values in Fig. 5. As shown, power consumption increases with cutting speed, depth of cut and feed rate. It can be concluded that power consumption is dependent

Table 3. Cutting conditions (Shao et al., 2004)

Groups	Number of teeth	Cutting of speed(m/min)	Depth of cut (mm)	Feed rate (mm/rev)	offset distance (mm)
1	1	18	4	0.8	0
2	5	94	4	0.8	0
3	5	94	5	0.78	0
4	5	149	2	1	0
5	5	149	3	1	0

on feed rate, f, cutting speed, ν, and depth of cut, a_p, in a descending order of correlation. Machine power consumption is most sensitive to feed rate for the system studied (and in the range of inputs studied). The impact of feed rate on power consumption is not affected by the tool wear. This sensitivity analysis helps us understand the relative impact of the parameters on power consumption.

Table 4. Data of cutting speed, depth of cut and feed rate form the work of Shao et al. (2004)

SerialNo.	Cutting speed $(\nu, m/min)$	Depth of cut (a_p, mm)	Feed rate $(f, mm/rev)$
1	18	4	0.8
2	94	4	0.8
3	94	5	0.78
4	149	2	1
5	149	3	1
Mean	100.8	3.6	0.876

5 Conclusions and Future work

A system model for milling processes was developed with the purpose of inferring power consumption from process parameters and system controlled variables. The model results are in good agreement with literature-reported experimental data. Sensitivity analysis was performed to explore the relationship of power consumption with system admissible inputs as a function of machining tool wear. Feed rate was shown to have the highest impact on the power consumption. Tool wear has a significant impact on machining power consumption, which is not constant across the operating envelop of the machine. On the other hand, the sensitivity of power consumption with respect to any of the considered system admissible inputs is similar in profile, regardless of tool wear. These insights will be drive decisions and interpretation of the sensor network design method described.

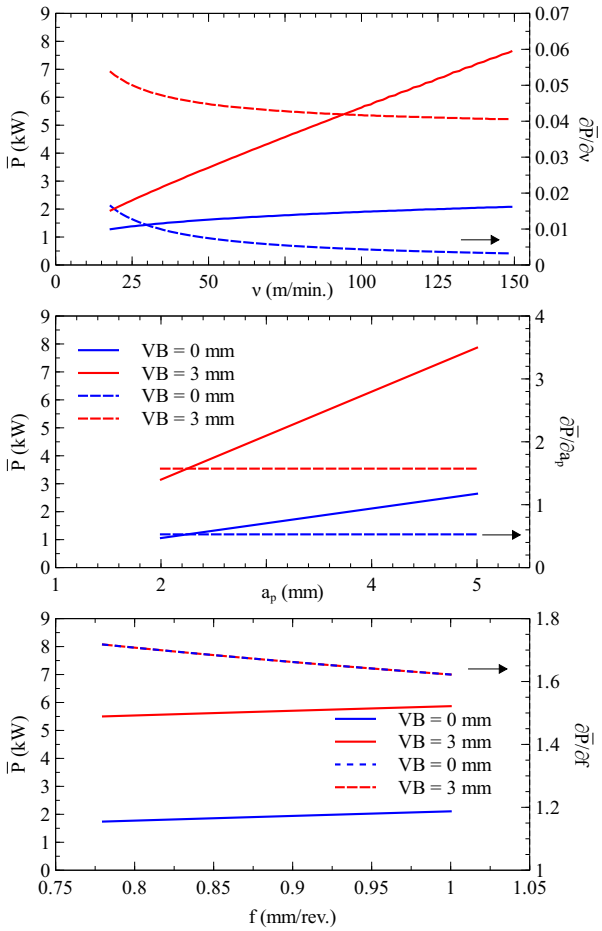

Fig. 5. Correlation between power and cutting speed (a), depth of cut (b), and feed rate (c).

References

Altintas, Y. (1988). In-process detection of tool breakages using time series monitoring of cutting forces. *International Journal of Machine Tools and Manufacture*, 28(2), 157 – 172.

Atkinson, A.C. and Bogacka, B. (1997). D- and Ds-optimum compound designs for the order of a chemical determining reaction. *Technometrics*, 39(4), 347–356.

Awasthi, U., Palmer, K.A., and Bollas, G.M. (2020). Optimal test and sensor selection for active fault diagnosis using integer programming (under review). *Journal of Process Control*.

Gutowski, T., Dahmus, J., and Thiriez, A. (2006). Electrical Energy Requirements for Manufacturing Processes. *Energy*, 2, 623–628.

Moradnazhad, M. and Unver, H.O. (2017). Energy efficiency of machining operations: A review. *Proceedings of the Institution of Mechanical Engineers, Part B: Journal of Engineering Manufacture*, 231(11), 1871–1889.

Munoz, A.A. and Sheng, P. (1995). An analytical approach for determining the environmental impact of machining processes. *Journal of Materials Processing Tech.*, 53(3-4), 736–758.

Palmer, K.A. and Bollas, G.M. (2019). Sensor selection embedded in active fault diagnosis algorithms. *IEEE Transactions on Control Systems Technology*, 1–14.

Palmer, K.A., Hale, W.T., and Bollas, G.M. (2019). Active fault identification by optimization of test designs. *IEEE Transactions on Control Systems Technology*, 27(6), 2484–2498.

Palmer, K.A. and Bollas, G.M. (2019a). Active fault diagnosis for uncertain systems using optimal test designs and detection through classification. *ISA Transactions*, 93, 354 – 369.

Palmer, K.A. and Bollas, G.M. (2019b). Analysis of transient data in test designs for active fault detection and identification. *Computers & Chemical Engineering*, 122, 93–104.

Shao, H., Wang, H.L., and Zhao, X.M. (2004). A cutting power model for tool wear monitoring in milling. *International Journal of Machine Tools and Manufacture*, 44(14), 1503–1509.

US Energy Information Administration (2011). *Annual Energy Review*.

Waldorf, D.J., Kapoor, S.G., and DeVor, R.E. (1992). Automatic recognition of tool wear on a face mill using a mechanistic modeling approach. *Wear*, 157(2), 305 – 323.